Liquid-crystalline coordination polymers based on tetra(alkoxybenzoato)dirhodium(II) complexes axially linked by tetrazine, phenazine and 4,4'-bipyridine

Leonardo Rossi, Cristián Huck-Iriart, María Ana Castro & Fabio D. Cukiernik

View supplementary material

Accepted author version posted online: 10 Nov 2017.
Published online: 23 Nov 2017.

Submit your article to this journal

Article views: 2

View related articles

View Crossmark data

Taylor & Francis
Taylor & Francis Group

Check for updates

Liquid-crystalline coordination polymers based on tetra(alkoxybenzoato)dirhodium(II) complexes axially linked by tetrazine, phenazine and 4,4'-bipyridine

Leonardo Rossi[a,b], Cristián Huck-Iriart[c,d], María Ana Castro[a,b] and Fabio D. Cukiernik[a,b]

[a]Facultad de Ciencias Exactas y Naturales, DQIAQF, Universidad de Buenos Aires, Buenos Aires, Argentina; [b]Instituto de Química Física de los Materiales, Medio Ambiente y Energía (INQUIMAE), CONICET- Universidad de Buenos Aires, Buenos Aires, Argentina; [c]Escuela de Ciencia y Tecnología, Universidad Nacional de San Martín, Provincia de Buenos Aires, Argentina; [d]Facultad de Ciencias Exactas, Departamento de Química, INIFTA, CONICET- Universidad Nacional de La Plata, La Plata, Argentina

ABSTRACT

The reaction of dirhodium tetrakis(3,4,5-trialkoxy)benzoates $Rh_2(B3OCn)_4$ (n = 10, 14, and 18) with three different dinitrogenated axial ligands (L_{ax}), namely tetrazine (tz), phenazine (phz), and 4,4'-bipyridine (bpy), gave rise to three homologous series of mesogenic coordination polymers, $[Rh_2(B3OCn)_4]L_{ax}$. All of them exhibited thermotropic columnar mesophases that were of the hexagonal type for tz and phz and rectangular for bpy. The lighter n = 10 homologs of the three series are liquid crystals (LC) at room temperature. Their mesomorphic properties have been compared with those of the previously studied L_{ax} = pyrazine series. Models for the supramolecular organization of the three polymeric series in their Col LC phases are proposed on the basis of their structural parameters, as measured by XRD and SAXS. The differences are interpreted in terms of different coordination features of the axial ligands.
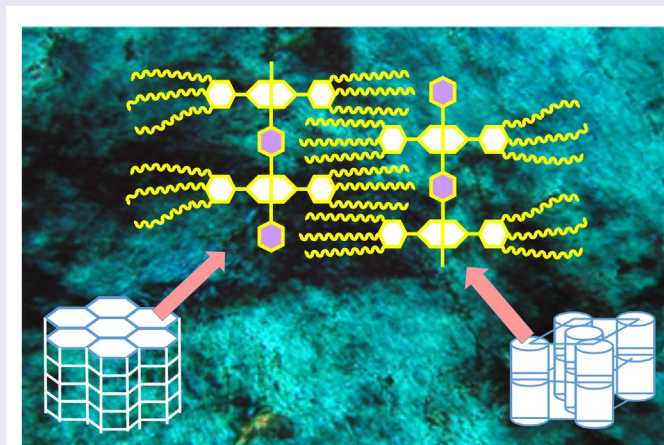
CONTACT Fabio D. Cukiernik ✉ fabioc@qi.fcen.uba.ar

Supplemental data for this article can be accessed at https://doi.org/10.1080/00958972.2017.1403594.

1. Introduction

Liquid crystals (LC) based on coordination polymers (LCCP) are an interesting class of materials among metallomesogens (metal-containing LC) due to their potential to combine typical properties of coordination polymers (CP) with the possibility of achieving orientation at a macroscopic scale from the (anisotropic) LC phase. Interesting examples have been reported in which the LC aggregation modifies specific properties of the CP like electrochromism [1], thermal stability [2], or magnetization [3, 4]. CP columnar mesophases are particularly attractive because of their potential charge or energy transport along the intermetallic 1-D axis of the columnar phase. In spite of the pointed potentiality, literature information about synthesis, characterization, and study of LC properties of LCCP remain scarce. Furthermore, a detailed correlation between LC properties and molecular structure of LCCP has not yet been established.

Most of the reported examples of columnar LCCP involve either *shish-kebab* metallophthalocyanines [5–7], vanadyl-β-diketonates [8], iron-containing triazole derivatives [9, 10], or CP of the MMX type like dirutheniumtetracarboxylates [11–14] and dirhodiumtetracarboxylates [15]. Although biphylic axial ligands provide a connection between metallic centers in those carboxylates (sometimes providing pathways for electronic communication along the metal centers), usually a void space is developed. This space precludes the organization of such CP as parallel columns in the crystalline phase [15–17], a prerequisite for the occurrence of higher temperatures Col_H LC phases [18, 19].

In previous works, we reported that an efficient strategy to overcome this problem is to fill the intermolecular space in an *intracolumnar* way: in the case of polymers of the $M_2(O_2CR)_4L_{ax}$ type (L_{ax} = bridging axial ligand), the use of bulky equatorial carboxylates like tri(alkoxy)benzoates proved successful. Indeed, the use of such equatorial ligands resulted in Col_H LC phases in the cases of M_2 = Ru_2(II,III) combined with L_{ax} = Cl⁻ [13, 17, 20] and M_2 = Rh_2(II,II) combined with L_{ax} = pyrazine (pz) [15]. In the present work, we extend that study on rhodium tri(alkoxy)benzoates to nitrogenated axial ligands with different coordination ability or geometric aspects (like N-to-N distance), namely tetrazine (tz), phenazine (phz), and 4,4'-bipyridine (bpy) (Scheme 1). We report the synthesis and characterization of these CP as well as the study of their LC properties. Some comparisons with bis-capped non-polymeric analogs [Rh_2(B3OCn)$_4$](phz)$_2$ (Scheme 1) as well as a plausible extension to Ru_2(II,II) analogs are also presented.
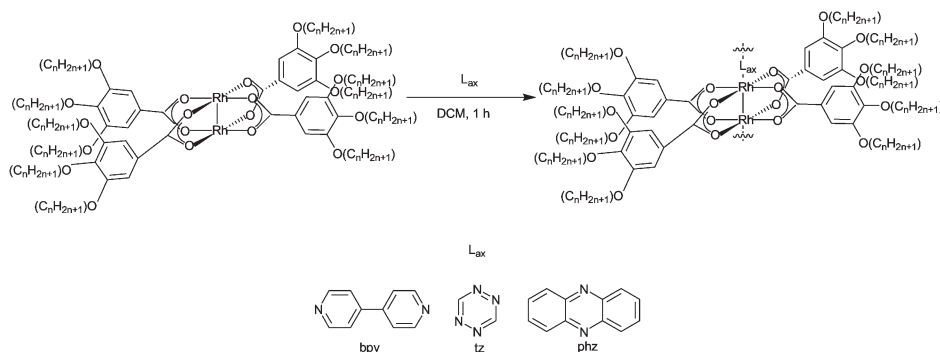
Scheme 1. General reaction diagram and chemical structure of involved compounds. Compounds will be hereafter noted as Rh2(B3OCn)4Lax, where "*n*" denotes the length (number of carbon atoms) of each aliphatic chain and "Lax" is the bridging axial ligand.

2. Experimental

2.1. Synthesis and characterization

All chemical precursors (rhodium acetate, gallic methyl ester, bromoalkanes, phenazine, 4,4′-bipyridine) were purchased from Sigma-Aldrich and used without purification except 1,2,4,5-tetrazine, which was synthesized according to a literature procedure [21]. Operations under inert atmosphere were carried out following Schlenck techniques. Purified solvents were provided by a *Puresolv* purifying apparatus.

IR spectra were recorded as thin films deposited on NaCl windows using a Nicolet FTIR 510P spectrometer. Elemental analyses were carried out at *Servicio a Terceros* of INQUIMAE on a Carlo Erba CHNS-O EA1108 analyzer. ^{1}H NMR spectra were measured at UMYMFOR on a Bruker AM500 spectrometer using $CDCl_3$ as solvent and its residual peaks as internal references (7.26 ppm for ^{1}H). UV–vis spectra were recorded using an HP8453 diode-array spectrophotometer.

The 3,4,5-tri(alkoxy)benzoic acids were synthesized by Williamson etherification of gallic methyl ester with the corresponding bromoalkanes, followed by basic hydrolysis, according to published procedures [13, 22]. Precursor complexes di(rhodium)tetrakis(3,4,5-trialkoxy-benzoates), noted as $Rh_2(3,4,5\text{-B3OC}n)_4$ ($n = 10$, 14, and 18), were prepared by metathesis reaction from rhodium acetate, as previously reported [15]; their nature and purity have been checked by FTIR, elemental analysis, and ^{1}H-NMR (see ESI).

Coordination polymers $Rh_2(3,4,5\text{-B3OC}n)_4L_{ax}$ have been synthesized by adding dropwise a dichloromethane (DCM) solution of the axial ligand (L_{ax} = tz, phz or bpy, 2 equivalents) to a DCM solution of the corresponding $Rh_2(3,4,5\text{-B3OC}n)_4$ precursor complex at room temperature (RT) with constant stirring. Detailed amounts of reactants and solvents used in each synthetic procedure, as well as their yields, are reported in Table S1. Experiments conducted with lower $[L_{ax}]/[Rh_2(3,4,5\text{-B3OC}n)_4]$ ratios gave rise to products with defect L_{ax}; molar ratios above this value gave rise to bis-adducts, which have also been synthesized, for L_{ax} = phz, under controlled conditions. Next steps for each of the synthesized compounds are described below.

2.1.1. $Rh_2(3,4,5\text{-B3OC}n)_4tz$ polymers

The initial green solution turned dark blue after tz addition. After stirring for 1 h, the solution was evaporated to dryness under reduced pressure. Excess tz was eliminated during this operation, as shown by the red vapors detected. The solid was then redissolved in DCM, and this dissolution/evaporation process was repeated until no tz vapors were detected. The resulting dark blue solids were dried under vacuum and afterward characterized by FTIR, ^{1}H-NMR, UV–vis, and elemental analysis, with yields above 80% in all cases. FTIR main bands (see a more complete description and assignment in the ESI): 2955, 2920, 2855 cm^{-1} (vCH$_2$, vCH$_3$) 1558 cm^{-1} (vCO$_2$^{assym}), 1409 cm^{-1} (vCO$_2$^{sym}), 1716 cm^{-1} ($v$tz) for the whole series. UV–vis: A broad band centered around 580 nm was observed, plus unresolved signals belonging to the aromatic rings (200–400 nm). ^{1}H-NMR (Figure S1): $\delta = 11.03/2H$ (broad, tz's H), $\delta = 7.20/8H$ (aromatic H from benzoates), $\delta = 3.83/24H$ (CH$_2$ α to the ether bond), $\delta = 1.70/24H$ (CH$_2$ β to the ether bond); $\delta = 1.39/24H$ (CH$_2$ γ to the ether bond); $\delta = 1.25$–$1.34/24$(n-4)H (other CH$_2$ nuclei); $\delta = 0.89/36H$ (terminal CH$_3$). Anal. Calcd for $Rh_2O_{20}N_2C_{150}H_{262}$ ($n = 10$, *catena*-[tetrakis(μ$_2$-3,4,5-tri(decyloxy)benzoato)dirhodium(II,II)]-μ$_2$-tetrazine)) (%): C, 68.0; H, 10.0; N, 2.1. Found: C, 67.8; H, 10.2; N, 1.9. Calcd for $Rh_2O_{20}N_2C_{198}H_{358}$ ($n = 14$,

catena-[tetrakis(μ_2-3,4,5-tri(tetradecyloxy)benzoato)dirhodium(II,II)]-μ_2-tetrazine) (%): C, 71.6; H, 10.8; N, 1.7. Found: C, 70.2; H, 11.1; N, 1.7. Calcd for $Rh_2O_{20}N_2C_{246}H_{454}$ ($n = 18$, *catena*-[tetrakis(μ_2-3,4,5-tri(octadecyloxy)benzoato)dirhodiu:m(II,II)]-μ_2-tetrazine) (%): C, 73.9; H, 11.5; N, 1.4. Found: C, 72.3; H, 11.6; N : 1.3.

2.1.2. *Rh$_2$(3,4,5-B3OCn)$_4$phz polymers*

The initial green solution turned red after phz addition. After stirring for 1 h, the solution was evaporated to dryness under reduced pressure. Excess phz was eliminated by rinsing the solid with cold methanol. The solid was then redissolved in DCM, and this dissolution/ evaporation process was repeated until no phz residue was detected in the methanol supernatant. The resulting solids were dried under vacuum and afterward characterized by FTIR, ^{1}H-NMR, UV–vis, and elemental analysis with yields above 90% in all cases. FTIR: 2955, 2920, 2855 cm^{-1} (νCH_2, νCH_3) 1563 cm^{-1} (νCO_2^{assym}), 1409 cm^{-1} (νCO_2^{sym}), 1720 cm^{-1} (νphz) for the whole series. UV–vis: A sharp band centered around 460 nm and another (broad) one at 600 nm were observed, plus unresolved signals belonging to the aromatic rings (200– 400 nm). ^{1}H-NMR (Figure S2a): Same as the Rh precursor complexes and tz polymers, except for the signals corresponding to coordinated phz: two sets of peaks at $\delta = 9.00/4H$ (broad, central H) and $\delta = 7.90/4H$ (sharp, lateral H). Anal. Calcd for $Rh_2O_{20}N_2C_{160}H_{268}$ ($n = 10$, *catena*-[tetrakis(μ_2-3,4,5-tri(decyloxy)benzoato)dirhodium(II,II)]-μ_2-phenazine) (%) : C, 70.0; H, 9.8; N, 1.0. Found: C, 69.3; H, 9.8; N, 0.9. (1.0). Calcd for $Rh_2O_{20}N_2C_{208}H_{364}$ ($n = 14$, *catena*-[tetrakis(μ_2-3,4,5-tri(tetradecyloxy)benzoato)dirhodium(II,II)]-μ_2-phenazine) (%) : C, 73.0; H, 10.7; N, 0.8. Found: C, 73.2; H, 10.9; N, 0.6. Calcd for $Rh_2O_{20}N_2C_{256}H_{460}$ ($n = 18$, *catena*-[tetrakis(μ_2-3,4,5-tri(octadecyloxy)benzoato)dirhodium(II,II)]-μ_2-phenazine)) (%): C, 75.1; H, 11.1; N, 0.7. Found: C, 74.1; H, 11.3; N, 1.0.

2.1.3. *Rh$_2$(3,4,5-B3OCn)$_4$(phz)$_2$ bis-capped monomers*

The same synthesis technique as the polymers, using 4 equivalents of phz, yielded crystalline powders. UV–vis: no significant changes from the polymers were observed, except for the fact that the broad band is centered at 570 nm. IR and ^{1}H-NMR spectra (Figure S2b) are very similar to those of the polymers, with sharper NMR peaks. Significant signals: $\delta = 8.75/8H$ (broad, central H) and $\delta = 7.90/8H$ (lateral H), 1565 cm^{-1} (νCO_2^{assym}), 1731 cm^{-1} (νtz). Calcd for $Rh_2O_{20}N_4C_{172}H_{276}$ ($n = 10$, [tetrakis(μ_2-3,4,5-tri(decyloxy)benzoato)dirhodium(II,II)]diphenazine) (%): C, 70.6; H, 9.5; N, 1.9. Found: C, 70.1; H, 9.6; N, 2.0. Calcd for $Rh_2O_{20}N_4C_{220}H_{372}$ ($n = 14$, [tetrakis(μ_2-3,4,5-tri(tetradecyloxy)benzoato)dirhodium(II,II)]diphenazine) (%): C, 73.4; H, 10.6; N, 1.5. Found: C, 73.0; H, 10.9; N, 1.3.

2.1.4. *Rh$_2$(3,4,5-B3OCn)$_4$bpy polymers*

The initial green solution turned to orange after bpy addition. After stirring for 1 h, the solution was evaporated to dryness under reduced pressure. Excess bpy was eliminated by rinsing the solid with cold methanol. The solid was then redissolved in DCM, and this dissolution/evaporation process was repeated until no bpy residue was detected in the methanol supernatant. The resulting solids were dried under vacuum and afterward characterized by FTIR, ^{1}H-NMR, UV-VIS and elemental analysis with yields above 90% in all cases. FTIR: 2955, 2920, 2853 cm^{-1} (νCH_2, νCH_3) 1558 cm^{-1} (νCO_2^{assym}), 1406 cm^{-1} (νCO_2^{sym}), 1726 cm^{-1} (νbpy) for the whole series. UV-Vis: A broad "shoulder" band centered around 400 nm and another, less intense at 560 nm were observed, plus unresolved signals belonging to the aromatic

rings (200–400 nm) ^{1}H-NMR (Figure S3): Same as starting Rh complexes, except axial ligand presents two sets of peaks at $\delta = 9.50/4H$ (broad, H closer to the bimetallic core) and $\delta = 8.30/4H$ (broad, other H). Calcd for $Rh_2O_{20}N_2C_{158}H_{268}$ ($n = 10$, catena-μ_2-[tetrakis(μ_2-3,4,5-tri(decyloxy)benzoato)dirhodium(II,II)](4,4'-bipyridine)) (%): C, 69.7; H, 9.9; N, 1.0. Found: C, 69.8; H, 10.0; N, 1.0. Calcd for $Rh_2O_{20}N_2C_{206}H_{364}$ ($n = 14$, catena-μ_2-[tetrakis(μ_2-3,4,5-tri(tetra-decyloxy)benzoato)dirhodium(II,II)](4,4'-bipyridine)) (%): C, 72.9; H, 10.8; N, 0.9. Found: C, 72.5; H, 10.6; N, 1.0.

2.2. Mesophase characterization

Mesomorphic behavior was studied by means of variable temperature polarizing optical microscopy (POM), differential scanning calorimetry (DSC), and variable temperature small angle X-ray scattering (SAXS) techniques as well as powder X-ray diffraction (PXRD) for room-temperature measurements. POM was carried out between crossed polarizers using a Leitz DMRX microscope equipped with a Leitz 1350 hot-stage. DSC experiments were performed on a Shimadzu DSC-50 calorimeter at a heating rate of 5 °C/min in all cases. PXRD experiments were performed at RT on a Siemens D5000 diffractometer (Siemens AG, Munich, Germany) using the K_α-copper radiation from a curved-graphite monochromator and planar glass sample holders.

SAXS experiments were performed at INIFTA facilities using a XEUSS equipment from XENOCS with a K_α-copper radiation microsource. A PILATUS-100 K detector was used with 513 mm sample detector distance. One-dimensional curves were obtained by integration of the 2-D data using the Foxtrot program. The scattering intensity distributions as a function of the scattering angle (2θ) were obtained in the 2θ range between 0.2 and 9.3°. The powdered samples were placed in a temperature controlled sample-holder from Linkam®. Each sample was contained between Kapton® windows and thermally stabilized ten minutes before measuring above RT.

3. Results

3.1. Synthesis and characterization

The reactions of $Rh_2(B3OCn)_4$ precursor complexes with tz, phz, and bpy were studied spectrophotometrically and were found to follow stepwise pathways. Figure 1 shows UV–vis spectra recorded for a DCM solution of $Rh_2(B3OC10)_4$ after addition of successive aliquots of tz (DCM solution). For low $[L_{ax}]/[Rh_2(B3OC10)_4]$ ratios (noted hereafter X), the original band at 655 nm progressively shifts to lower energies, reaching $\lambda_{max} = 695$ nm for $X = 0.5$. This band then shifts back –with isosbestic point at 648 nm for higher $[L_{ax}]/[Rh_2(B3OC10)_4]$ ratios, reaching $\lambda_{max} = 588$ nm for $X = 1$. For higher X values, this band remains unchanged. The band located at 420 nm for the parent complex progressively overlaps with a new intense one at 380 nm, whose intensity decreases for X values between 0.5 and 1.0, then remains unchanged. Spectra for X values higher than 2 are dominated by the absorption of free tetrazine and are not informative.

A plot of the corrected absorbance at each of the stated wavelengths versus $X = [L_{ax}]/[Rh_2(B3OC14)_4]$ ratio (Figure 2) shows the first reaction proceeds through a 1 : 2 stoichiometry. This corresponds to the formation of a dimer of binuclear units according to Equation (1);
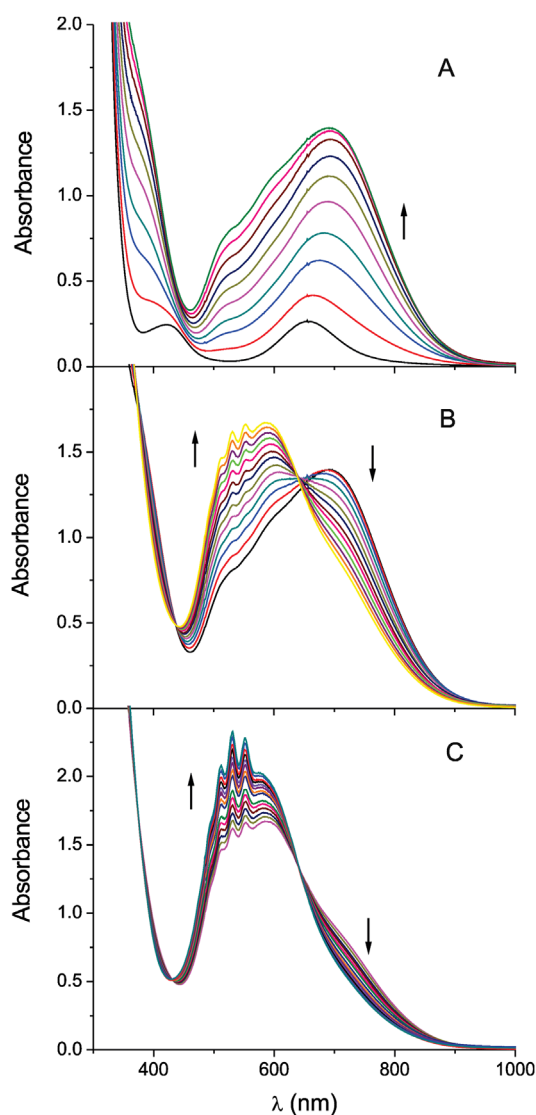
Figure 1. UV–vis spectrophotometric titration of $Rh_2(B3OC10)_4$ with tz in dichloromethane solution. (A) $0 < X < 0.54$, (B) $0.54 < X < 1.25$, (C) $1.25 < X < 2$.

the second one, with a global 1 : 1 stoichiometry, corresponds to the formation of polymeric/oligomeric species according to Equation (2) (for simplicity $Rh_2(B3OCn)_4$ is referred to as $[Rh_2]$):

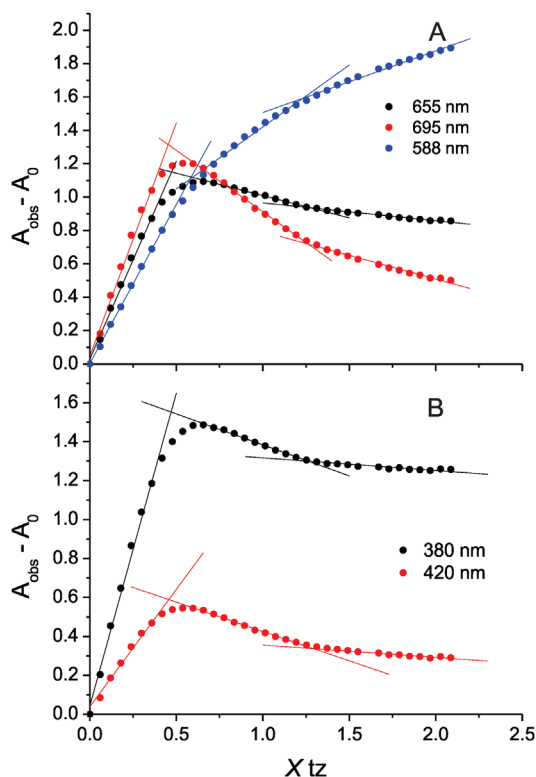$$2[Rh_2] + tz \rightarrow [Rh_2]\text{-tz-}[Rh_2] \qquad (1)$$

$$n/2[Rh_2]\text{-tz-}[Rh_2] + n/2\ tz \rightarrow ([Rh_2]\text{-tz-})_n \qquad (2)$$
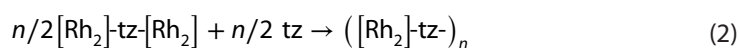
Figure 2. Job's plot for the titration of $Rh_2(B3OC10)_4$ with tz following λ_{max} (A) 655, 695, and 588 nm; (B) 380 and 420 nm.

A_{obs}: observed absorbance; A_0 = absorbance for the free complex. Linear fits for the different regions were used to determine the intersections.

In turn, these species transform in the bis-capped binuclear units ("bis-aducts") at higher $[L_{ax}]/[Rh_2(B3OCn)_4]$ ratios according to Equation (3) and the whole stepwise pathway is schematically represented in Scheme 2.

$$\left([Rh_2]\text{-tz-}\right)_n + n\ tz \rightarrow n\ tz\text{-}[Rh_2]\text{-tz} \tag{3}$$
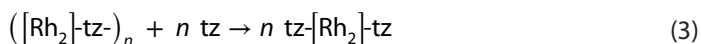
Similar results (Figure S4) were obtained for bpy axial ligand, with $\lambda_{max} = 562$ nm for $[Rh_2]$-bpy-$[Rh_2]$ and 518 nm for $([Rh_2]$-bpy-$)_n$. In this case, both reactions proceed with defined isosbestic points at 600 and 540 nm, respectively; the absence of strong absorption bands
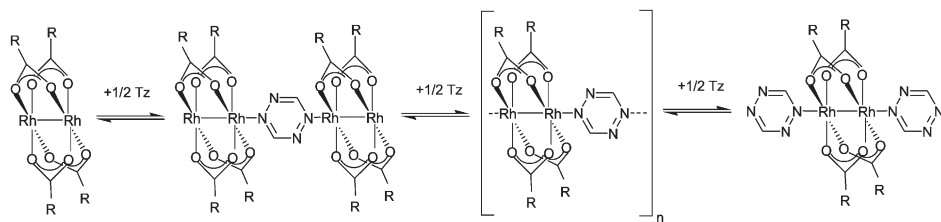
Scheme 2. General stepwise pathway for the formation of monomeric, dimeric, and polymeric species.

due to free bpy in the vis region allowed for a complete titration up to $X = 4$. The same kind of spectrophotometric titration with phz yielded slightly different results: the original band at 660 nm decreases while a new one at 600 nm increases. However, Job's plot shows this reaction proceeds through a 1 : 1 stoichiometry (Figure S5), suggesting direct formation of $([Rh_2]\text{-phz-})_n$ species without evidence of formation of $[Rh_2]$-phz-$[Rh_2]$ dimers of binuclear units. Usual treatment [23] of the A_{corr} versus X allows for the determination of the constant equilibrium for (1), K_1. We obtained K_1 values of 2×10^9 for tz and 2.5×10^7 for bpy. The corresponding value for pz, recalculated from previously published data [15], is 8×10^{10}. This tendency does not correlate with the basicity of L_{ax}, but certainly reflects the result of competing σ-bond, π-backbond, and electrostatic factors.

The fact that the L_{ax} complexation is not quantitative for stoichiometric ratios prompted us to synthesize the target $[Rh_2(B3OCn)_4]L_{ax}$ polymers using an excess of L_{ax} during the synthesis. Following this synthetic route, all polymers were obtained with good yield and purity. They are all air-stable although they decompose in solution in a matter of days to yield brown solutions. In addition to the already discussed UV–vis evidence, ^1H-NMR proved the actual coordination of the axial ligand: in all cases, H nuclei of L_{ax} located near the central polymer axis appeared as broad, flat signals shifted to lower fields than in the free L_{ax}. This was particularly evident for phz compounds, where two sets of signals were present: one sharp slightly shifted (+0.05 ppm) from free phz, and the other broad and greatly shifted downfield (+0.75 ppm). IR spectra of all the synthesized polymers and bis-capped complexes are almost identical to those of the parent compounds, with νCO_2^{assym} (1548 cm^{-1} in the parent complexes) slightly shifted to higher frequencies. The similarity in the spectra of both kinds of compounds confirms the paddlewheel cores remained intact during polymer formation. Unfortunately, symmetric stretching modes of the axial ligands, expected in the 1580–1600 cm^{-1} region, which have been useful in the past for establishing the bridging or terminal character of pyrazine or 4,4'-bpy in other coordination polymers [24, 25], are here obscured by other bands assigned to $Rh_2(O_2Car)_4$ modes. A band around 1700–1730 cm^{-1} could be detected for both polymers (weak) and bis-capped phz compounds (medium intensity); it might be ascribed to combinations of fundamental modes of the axial ligands themselves [26] or with fundamental modes of the binuclear units.

3.2. Liquid crystalline properties

The phase sequence, thermal, and structural parameters found for each of the studied compounds are summarized in Table 1 and analyzed below. Detailed information about the structural characterization of each compound can be found in Table S3 (ESI); comprehensive descriptions of the different types of CLC phases (hexagonal, rectangular, tetragonal) can be found in Refs. [27, 28].

3.2.1. Tetrazine derivatives

The three studied polymers $Rh_2(B3OCn)_4$tz exhibited a thermotropic Col_H phase, after the birefringent textures observed under POM and the $1: \sqrt{3}: \sqrt{4}$ progression found in their XRD or SAXS patterns (Figure 3 and Table 1); the former also showed the characteristic broad halo at ca. 20° (4.5 Å, molten aliphatic chains). These Col mesophases were found to be present even at room temperature for the $n = 10$ and 14 derivatives and above 59 °C for the $n = 18$ homolog.

Table 1. Phase sequence and parameters for all the studied compounds.

Compound	Mesomorphism and phase sequence[a]	Mesophase parameters[b]
$Rh_2(B3OC10)_4tz$	$Col_h \cdot 230 \cdot I + Dec$	$a = 28.0$ Å $S = 678$ Å^2 $V = 3740$ Å^3
$Rh_2(B3OC14)_4tz$	$Col_h \cdot 240 \cdot I + Dec$	$a = 32.7$ Å $S = 923$ Å^2 $V = 5091$ Å^3
$Rh_2(B3OC18)_4tz$	$Cr \cdot 59 (103) \cdot Col_h \cdot 260 (26) \cdot I + Dec$	$a = 36.1$ Å $S = 1130$ Å^2 $V = 6233$ Å^3
$Rh_2(B3OC10)_4phz$	$Col_h \cdot 240 \cdot I+Dec$	$a = 28.6$ Å $S = 709$ Å^2 $V = 3622$ Å^3
$Rh_2(B3OC14)_4phz$	$Cr \cdot 62 (24) \cdot Col_h \cdot 267 \cdot I+Dec$	$a = 33.7$ Å $S = 985$ Å^2 $V = 5032$ Å^3
$Rh_2(B3OC18)_4phz$	$Cr \cdot 75 (314) \cdot Col_h \cdot 300 (77) \cdot I+Dec$	$a = 37.2$ Å $S = 1197$ Å^2 $V = 6115$ Å^3
$Rh_2(B3OC10)_4(phz)_2$	$Cr \cdot 52 (70) \cdot I\ Col_h\ (*)$	$a = 26.8$ Å $S = 830$ Å^2
$Rh_2(B3OC14)_4(phz)_2$	$Cr \cdot 65 (171) \cdot I\ Col_h\ (*)$	$a = 36.7$ Å $S = 1163$ Å^2
$Rh_2(B3OC10)_4bpy$	$0 \cdot Col \cdot 273 \cdot I+Dec$	$(-)$
$Rh_2(B3OC14)_4bpy$	$Cr \cdot 69 (171) \cdot Col_r \cdot 285 \cdot I+Dec$	$a = 53$ Å $b = 33.8$ Å $S = 1792$ Å^3 $V = 23,296$ Å^3

(*)Monotropic Col_h mesophases detected on cooling.

[a]Cr = crystalline, Col_h = columnar hexagonal, Col_r = columnar rectangular, I = Isotropic, Am = amorphous, Dec = decomposition. Transition temperatures in °C; transition enthalpies (in parenthesis) in kJ/mol.

[b]a: length of the unit cell parameter for the hexagonal columnar mesophases; a and b: length of the unit cell parameters for the rectangular columnar mesophases; S: unit cell surface; V volume of one columnar section of surface S, and height h ($V = S.h$; h calculated as explained in the text).

3.2.2. Phenazine derivatives

Brighter POM textures as well as SAXS or XRD patterns exhibiting peaks in a $1: \sqrt{3}: \sqrt{4}: \sqrt{7}$ reciprocal ratio in addition to a broad halo at *ca.* 20° (Figure 4 shows those corresponding to $Rh_2(B3OC10)_4phz$ as an example) pointed to Col_H mesophases being also present for polymeric $Rh_2(B3OCn)_4phz$ compounds. Also, DSC studies showed they exhibited a narrower range than that found for the tz analogs. Interestingly, virgin samples of $Rh_2(B3OC10)_4(phz)_2$ and $Rh_2(B3OC14)_4(phz)_2$ bis-adducts exhibited a crystalline phase at RT but upon heating to the isotropic phase and slowly cooling back to RT, a monotropic Col_H mesophase was formed (Figure 5).

3.2.3. 4,4′-Bipyridine derivatives

The thermal behavior of $Rh_2(B3OC10)_4bpy$ and $Rh_2(B3OC14)_4bpy$ is similar to that found for the same analogs of the previous series. However, their mesophases exhibit (Figure 6) brighter POM textures as well as SAXS patterns that differ from those recorded for the previously analyzed polymers. Indeed, SAXS for $n = 10$ homolog exhibits just a broad peak centered at *ca.* 3° followed by a weak peak (seen as a shoulder) at *ca.* 4.5°. These values are compatible with a tetragonal array, although no clear assignments could be made. For $n = 14$, the SAXS pattern recorded in the mesophase exhibits several peaks, which could be indexed as the 11, 20, 02, 31, 22, and 04 reflexions of a rectangular *C2/m* lattice (Table 1). The last
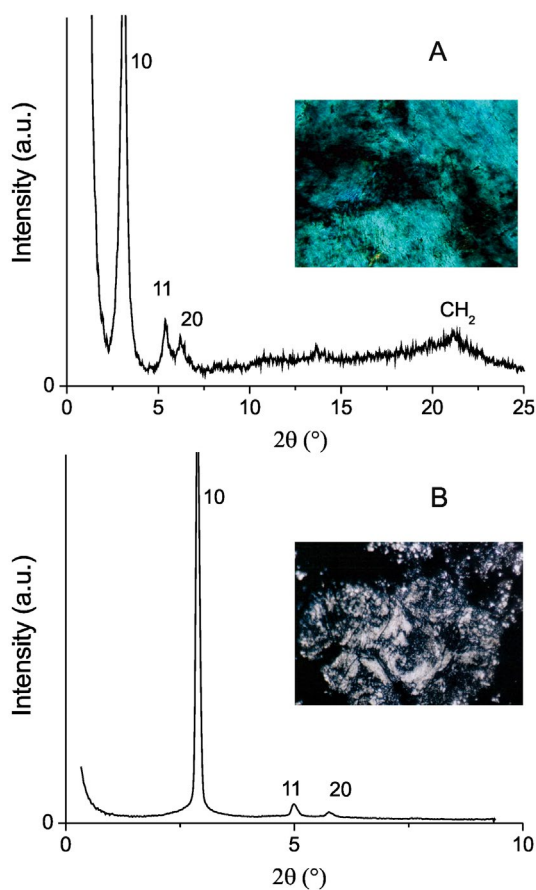
Figure 3. Characterization of the mesophases exhibited by $Rh_2(B3OCn)_4tz$ compounds. (A) XRD at RT for $n = 14$. (B) SAXS profile at 80 °C for $n = 18$. In both cases POM textures at the same temperatures are shown.

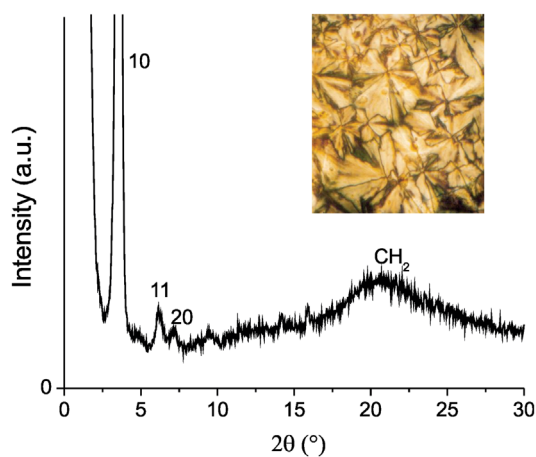**Figure 4.** RT XRD pattern for $Rh_2(B3OC10)_4phz$ with peaks indexed in an hexagonal system. The POM texture was taken after heating to the isotropic phase and slowly cooling back to RT.
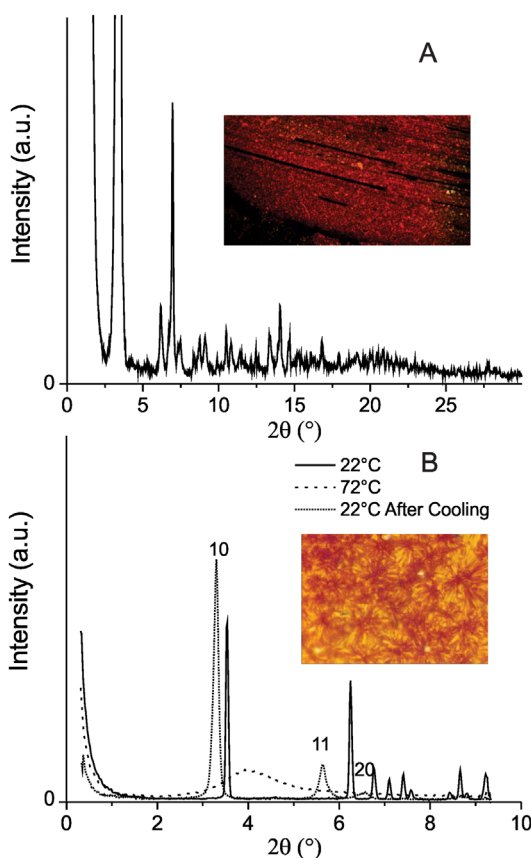
Figure 5. (A) Room temperature XRD pattern and POM texture of a virgin sample of the $Rh_2(B3OC10)_4(phz)_2$ bis-capped monomer. (B) SAXS for the same sample at varying temperatures, and corresponding POM image after reaching the isotropic state then cooling back to room temperature.

reflexion of this progression appears at $2\theta = 6.68°$ (13.2 Å) as the lower component of two overlapped peaks; we assign the highest component with maximum at 6.80° (*ca*. 13.0 Å) as the intracolumnar repeat distance, *h* (see below).

4. Discussion

In order to gain insight on the supramolecular organization of the studied polymers in their respective mesophases, the structural analysis will include data of the previously reported $[Rh_2(B3OCn)_4]$pz series, as well as a comparison to the parent complexes. We will first focus the discussion on the Col_H mesophases found for the $[Rh_2(B3OCn)_4]$tz, $[Rh_2(B3OCn)_4]$phz, and $[Rh_2(B3OCn)_4]$pz polymers as well as their $Rh_2(B3OCn)_4$ precursors. The unit cell surface (S) of the respective hexagonal mesophases is plotted against the chain length (*n*) in Figure 7 for all the four series under analysis. In all cases, S increases linearly with *n*. However, the columnar surfaces for the compounds of the pz series are smaller than those of the parent complexes whereas those of the tz and phz series are higher.
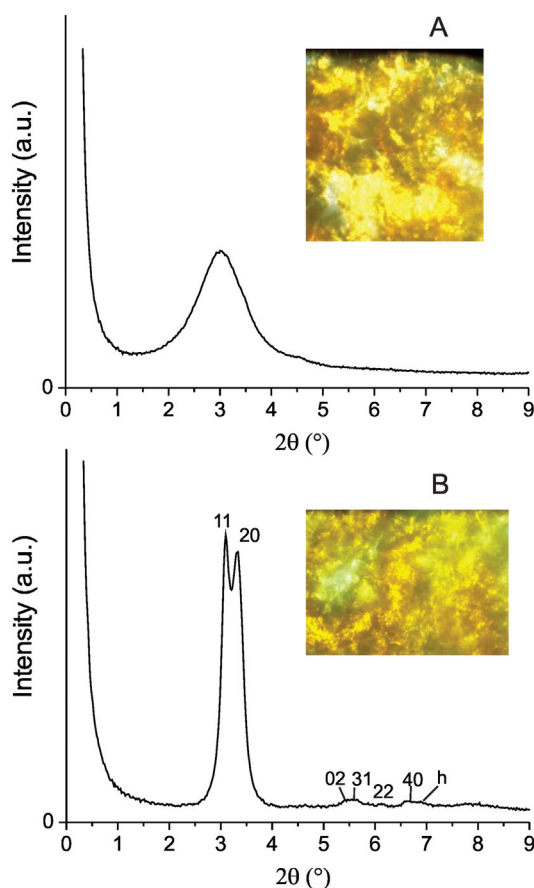
Figure 6. (A) Room temperature SAXS pattern and POM texture for $Rh_2(B3OC10)_4bpy$. (B) SAXS pattern at 89 °C and POM texture after heating and cooling to room temperature for $Rh_2(B3OC14)_4bpy$.

The fact that the pyrazine polymers exhibited a lower columnar surface than the parent compounds had been ascribed to the void space around the small axial pyrazine ligand [15]. This void space can be filled either by interdigitated aliphatic chains belonging to neighboring polymer strands or by strongly coiled aliphatic chains of the binuclear units linked to the pyrazine moiety in the same strand; both situations give rise to a contraction of the columnar surface compared to that of the parent compound. However, the measured intracolumnar repeats distance points to the latter suggestion being more plausible. Unexpectedly, the columnar surfaces measured for the tetrazine and phenazine polymers are higher than those of the parent compounds (and higher than those of the pyrazine analogs by a factor of *ca.* 1.7). One possible explanation might be that each column is built up by more than one polymeric strand, a fact already found in LCCP based on diruthenium tetracarboxylates [11, 19] and dirhodium tetrabenzoates $Rh_2(B2OCn)_4$ [15].

The plausibility of this explanation can be assessed following a usual approach in the structural analysis of columnar mesophases [11, 29, 30]. The volume of one columnar repeat unit, centered on one node of the hexagonal array, with transversal section area S and height h can be expressed as:
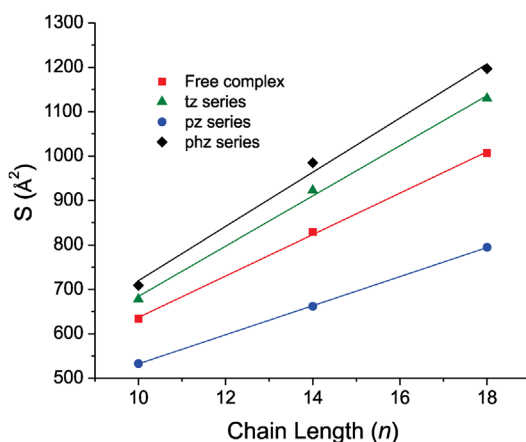
Figure 7. Plot of Unit Cell Surface (S) *vs.* chain length (*n*: number of carbon atoms in each aliphatic side chain) for the four series exhibiting Col$_H$ mesophases. Symbols represent the experimental data: (■) parent compounds (data taken from Ref. [15]), (▲) tetrazine series, (●) pyrazine series (data taken from Ref. [15]), (◆) phenazine series) and the continuous line is the result of a linear fitting procedure.

$$V = Sh = pV_o \tag{4}$$

where V_o is the volume of one binuclear unit (including the axial ligand) and p the number of such binuclear units within the columnar section. Under the assumption of complete filling of the space and the hypothesis of additivity of partial volumes, the volume V_o can be written as:

$$V_o = V_{rc} + 12 \times \left[n \times VCH_2 + \Delta VCH_3 \right] \tag{5}$$

In this equation, V_{rc} is the volume of the rigid core corresponding to the skeleton of the coordination polymer, including both one $[Rh_2(O_2CC_6H_2O_3)_4]$ unit and one molecule of the axial ligand, assumed to remain constant with n, 12 stands for the number of aliphatic chains (*n* carbon atoms each) in each binuclear unit, and ($n \times VCH_2 + \Delta VCH_3$) is the volume of one aliphatic chain *n* carbon atoms long. Combining Equations (4) and (5), the unit cell surface is expected to vary linearly with *n* according to Equation (6):

$$S = (p/h) \times \left[V_{rc} + 12 \times \Delta VCH_3 \right] + (p/h) \times \left[12 \times VCH_2 \right] \times n \tag{6}$$

Parameters obtained from linear regressions on data of Figure 7 are collected in Table 2; h/p values have subsequently been calculated using $VCH_2 = 25.97$ Å^3 for tz and phz series (data at room temperature) [31] and 26.03 Å^3 for pz series (data at 100 °C).

The h/p value found for the pyrazine series agrees well with the reported distances (9.55–9.60 Å) found in the crystalline structures of several CP in which the dirhodium tetrabenzoate units are polymerized by pyrazine or pyrazine derivatives (CSD refcodes NIKXEL, XUVMOQ, KELDAH, LUSVUR, LUSWEC, YILDUT, YILFAB). This distance is slightly shorter than the sum of the individual Rh-Rh, Rh-N, and N⋯N distances due to a bent conformation [15] along the CP; nevertheless, this value is a clear indication that each columnar section contains only

Table 2. Structural parameters arising from linear regressions for each of the four series exhibiting Col_h mesophases.

Parameter	Complex	pz	Tz	Phz
Slope (Å^2)	46.6	32.8	56.5	61.0
Intercept (Å^2)	171	205	119	110
h/p (Å)	6.7	9.5	5.5	5.1

one molecular unit ($p = 1$), then each column contains just one CP strand in $Rh_2(B3OCn)_4$pz compounds. However, the h/p values calculated for the other two CP series are too short to be assigned straightforward to the intracolumnar repeat distances. Indeed, the Rh···Rh' distance found in the two reported crystalline structures of rhodium (substituted)benzoates polymerized with phz (CSD refcodes ZICKAZ, ZOKNIY) lies in the range 9.57–9.90 Å (9.3–10.0 including some Ru analogs ZICJOM and KUKMOS). No direct comparison could be made with tz analogs as no crystalline structures of $M_2(RCO_2)_4$tz compounds have been reported; however, an estimation made on the basis of the reported structures of other transition metal complexes linked by tetrazine (RIFDRO, YOYTIQ, YOYTUC, YOYTAI) predicts M···M' distances longer than 9.0 Å. Consequently, for these two series, p must certainly be 2, in agreement with their higher unit cell surfaces. The intrastrand repeat distances h are thus 10.2 Å for the phenazine series and 11.0 Å for the tetrazine series. These values point to an interdigitated organization of the polymeric strands inside each column, as depicted in Figure 8 and already reported for CP based on ruthenium tetracarboxylates.

The difference between the kind of organization of the pz series ($p = 1$, no interdigitation) and the phz and tz series ($p = 2$, interdigitation) seems to be related to the M···M' intrastrand repeat distances (h): longer distances seem to allow for interdigitation whereas shorter distances seem to avoid interdigitation. This argument finds support in the two reported crystalline structures containing phz as axial ligand (and very similar equatorial ligands), where a longer M···M' distance was found for the interdigitated system (ZICKAZ) while a shorter one for the non-interdigitated one (ZOKNIY). The ability of a given $Rh_2(B3OCn)_4L_{ax}$ system to adopt longer M···M' distances could, in turn, be related to the Rh···L_{ax} bond strength. Indeed, pz axial ligand yielded the shorter h distances and the higher K_1 values, tz, and phz yielded longer distances and a lower Rh_2···L_{ax} affinity.

Compounds containing bpy as axial ligand were not included in the previous analysis for two reasons: first, they exhibited LC phases which differ from the Col_h found in the three series just discussed; second, bpy is a ligand significantly longer than pz, tz, and phz. The LC
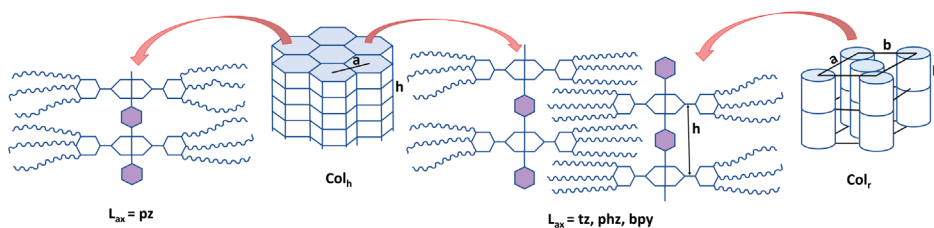
Figure 8. Schematic representation of the suggested models for the supramolecular organization of the columnar mesophases of the different $Rh_2(B3OCn)_4L_{ax}$ coordination polymers for L_{ax} = pz, tz, phz, and bpy. Purple hexagons represent L_{ax}.

phase of $Rh_2(B3OC10)_4$bpy seems to exhibit some kind of tetragonal array, although no further conclusions about its supramolecular organization can be drawn. However, the LC phase of $Rh_2(B3OC14)_4$bpy could clearly been assigned as a *C2/m* Col_R mesophase. As stated below, the peak found at 6.80°, which do not belong to the progression of the rectangular lattice, has been assigned to h, an intracolumnar repeat distance of 13.0 Å. This value is fully consistent with, for example, the $M \cdots M'$ distance (13.85 Å) found in the crystalline structure of Rh_2(pivalate)$_4$bpy (refcode LIJCIQ) [32]. Although we cannot derive in the present case an h/p value from the dependence of S with n, as in the previous series, p should be certainly taken as 2 for the compound under analysis due to the high S value found for the rectangular unit cell. As an additional evidence for the suggested model, the experimental density of $Rh_2(B3OC14)_4$bpy, measured by the floatation method [33], was found to be 0.88 ± 0.02 g/cm^3, in close agreement with the calculated one (0.95 g/cm^3) within the usually accepted uncertainties.

5. Conclusions and perspectives

We extended the family of previously reported Rh_2(II,II) tetra(alkoxy)benzoate coordination polymers, while maintaining the LC character. The kind of supramolecular organization in the LC phase depends on subtle differences in the coordinating features of L_{ax}. All CP containing axial ligands bearing the two coordinating N atoms at the opposite positions of the same aromatic ring (L_{ax} = pz, tz, and phz) and tridecyloxybenzoates ($n = 10$) as equatorial ligands showed Col_h mesophases at room temperature; heavier homologs exhibited Col_h mesophases at higher temperatures. Bpy derivatives exhibited more complex mesophases due to the different packing arrangements arising from longer $M \cdots M'$ distances. In all cases, the mesophase remains after cooling to room temperature from above $T_{transition}$. From the viewpoint of the molecular design of materials exhibiting specific LC features, once the L_{ax} is adequately chosen for yielding a Col_H phase, transition temperatures can be tuned by modulating the side chain length.

CP where bimetallic centers are axially linked by communicating ligands like those studied here could yield interesting physical properties, like charge migration along the CP axis. Among the studied L_{ax}, tetrazine appears as the most promising one: the ability of tz to connect metallic centers and to promote electron migration has been clearly established for both dinuclear compounds [34] and CP based on phthalocyanines [35], the key factor being the energy matching between tz and the metallic centers. As the electronic structure of Rh_2(II,II) carboxylates involves closed-shell units [36], we cannot expect significant electron migration via delocalization along the CP axis. However, their Ru_2(II,II) analogs bear 4 electrons in the 3-fold degenerate HOMO [36, 37], being thus suitable for such a property. Indeed, we computationally predicted [38] that among CP based on bimetallic carboxylates, Ru_2(II,II) units axially linked by tz are expected to exhibit the highest degree of electron delocalization. On the other hand, in order to perform these measurements along the CP axis (an even to think about eventual applications), it is necessary to obtain samples in which a given macroscopic direction could be associated with the CP axis. The CLC character of the CP could be exploited to yield such an orientation, for example, by extruding oriented fibers from the CLC phase. Indeed, we synthesized and characterized some Ru_2(II,II)/tz analogs of the Rh_2(II,II) CP reported here, extruded them from the CLC phase as oriented fibers, and measured their electric conductivity along the fiber axis. Although the detailed results will be the subject

of a specific report [39] we can preliminarily anticipate here that such oriented fibers exhibited high conductivities (*ca.* 10^{-1} Siemens/m), see Supporting Information). We should point out that both the synthetic conditions needed to obtain such Ru/CP and the structure of their CLC phase were slightly different from those of their respective Rh/CP counterparts. This observation is in line with the subtle effect of L_{ax} nature on the stability and LC properties of $M_2(O_2CR)_4$ CP found in this work.

Acknowledgements

Disclosure statement

No potential conflict of interest was reported by the authors.

Funding

References

[1] R. Kuwahara, S. Fujikawa, K. Kuroiwa, N. Kimizuka. *J. Am. Chem. Soc.*, **134**, 1192 (2012).
[2] M.C. Rusjan, E.E. Sileo, F.D. Cukiernik. *Solid State Ion.*, **124**, 143 (1999).
[3] Y. Bodenthin, G. Schwarz, Z. Tomkowicz, T. Geue, W. Haase, U. Pietsch, D.G. Kurth. *J. Am. Chem. Soc.*, **131**, 2934 (2009).
[4] M. Seredyuk, A.B. Gaspar, V. Ksenofontov, Y. Galyametdinov, M. Verdaguer, F. Villain, P. Gütlich. *Inorg. Chem.*, **47**, 10232 (2008).
[5] M. Hanack, A. Beck, H. Lehmann. *Synthesis*, **1987**, 703 (1987).
[6] A.P.M. Kentgens, B.A. Markies, J.F. Van der Pol, R.J.M. Nolte. *J. Am. Chem. Soc.*, **112**, 8800 (1990).
[7] T. Sauer. *Macromolecules*, **26**, 2057 (1993).
[8] W. Haase, D. Kilian, M.A. Athanassopoulou, D. Knawby, T.M. Swager, S. Wróbel. *Liq. Cryst.*, **29**, 133 (2002).
[9] M. Seredyuk, A.B. Gaspar, V. Ksenofontov, S. Reiman, Y. Galyametdinov, W. Haase, E. Rentschler, P. Gütlich. *Chem. Mater.*, **18**, 2513 (2006).
[10] T. Fujigaya, D.L. Jiang, T. Aida. *J. Am. Chem. Soc.*, **127**, 5484 (2005).
[11] T. Bottazzi, F. Cecchi, A. Zelcer, B. Heinrich, B. Donnio, D. Guillon, F.D. Cukiernik. *J. Coord. Chem.*, **66**, 3380 (2013).
[12] J.F. Caplan, C.A. Murphy, S. Swansburg, R.P. Lemieux, T.S. Cameron, M.A. Aquino. *Can. J. Chem.*, **76**, 1520 (1998).
[13] Z.D. Chaia, M.C. Rusjan, M.A. Castro, B. Donnio, B. Heinrich, D. Guillon, R.F. Baggio, F.D. Cukiernik. *J. Mater. Chem.*, **19**, 4981 (2009).
[14] F.D. Cukiernik, P. Maldivi, A.M. Giroud-Godquin, J.C. Marchon, M. Ibn-Elhaj, D. Guillon, A. Skoulios. *Liq. Cryst.*, **9**, 903 (1991).
[15] M. Rusjan, B. Donnio, D. Guillon, F.D. Cukiernik. *Chem. Mater.*, **14**, 1564 (2002).
[16] J. Barbera, M.A. Esteruelas, A.M. Levelut, L.A. Oro, J.L. Serrano, E. Sola. *Inorg. Chem.*, **31**, 732 (1992).

[17] F.D. Cukiernik, M. Ibn-Elhaj, Z.D. Chaia, J.C. Marchon, A.M. Giroud-Godquin, D. Guillon, A. Skoulios, P. Maldivi. *Chem. Mater.*, **10**, 83 (1998).

[18] G.S. Attard, P.R. Cullum. *Liq. Cryst.*, **8**, 299 (1990).

[19] M. Ibn-Elhaj, D. Guillon, A. Skoulios, A.M. Giroud-Godquin, P. Maldivi. *Liq. Cryst.*, **11**, 731 (1992).

[20] M. Rusjan, B. Donnio, B. Heinrich, F.D. Cukiernik, D. Guillon. *Langmuir*, **18**, 10116 (2002).

[21] J. Sauer, D.K. Heldmann, J. Hetzenegger, J. Krauthan, H. Sichert. *Eur. J. Org. Chem.*, **1998**, 2885 (1998).

[22] H. Strzelecka, C. Jallabert, M. Veber, J. Malthete. *Mol. Cryst. Liq. Cryst. Inc. Nonlinear Opt.*, **156**, 347 (1988).

[23] C.N. Reilley, D.T. Sawyer. In *Experiments for Instrumental Methods*, Robert E. Krieger (Ed.), Publishing Company, Inc., (1979).

[24] J.P. Collman, J.T. McDevitt, G.T. Yee, M.B. Zisk, J.B. Torrance, W.A. Little. *Synth. Met.*, **15**, 129 (1986).

[25] J. Metz, O. Schneider, M. Hanack. *Spectrochim. Acta, Part A*, **38**, 1265 (1982).

[26] R.C. Lord, A.L. Marston, F.A. Miller. *Spectrochim. Acta*, **9**, 113 (1957).

[27] S. Laschat, A. Baro, N. Steinke, F. Gieselmann, C. Haegle, G. Scalia, R. Judele, E. Kapatsina, S. Sauer, A. Schreivogel, M. Tosoni. *Angew. Chem. Int. Ed. Engl.*, **46**, 4812 (2007).

[28] T. Wöhrle, I. Wurzbach, J. Kirres, A. Kostidou, N. Kapernaum, J. Litterscheidt, J.C. Haenle, P. Staffeld, A. Baro, F. Giesselmann, S. Laschat. *Chem. Rev.*, **116**, 1139 (2016).

[29] D. Guillon. In *Liquid Crystals II, Vol. 95 of "Structure and Bonding"*, pp. 41–82, Springer, Berlin (1999).

[30] A.M. Levelut. *J. chim. Phys.*, **80**, 149 (1983).

[31] D. Guillon, A. Skoulios, J.J. Benattar. *J. Phys.*, **47**, 133 (1986).

[32] M. Handa, M. Watanabe, D. Yoshioka, S. Kawabata, R. Nukada, M. Mikuriya, H. Azuma, K. Kasuga. *Bull. Chem. Soc. Jpn.*, **72**, 2681 (1999).

[33] E.A. Hughes, H.M. Ceretti, A. Zalts. *J. Chem. Educ.*, **78**, 522 (2001).

[34] M. Glöckle, W. Kaim, A. Klein, E. Roduner, G. Hübner, S. Zalis, J. van Slageren, F. Renz, P. Gütlich. *Inorg. Chem.*, **40**, 2256 (2001).

[35] M. Hanack, M. Lang. *Adv. Mater.*, **6**, 819 (1994).

[36] J.G. Norman, G.E. Renzoni, D.A. Case. *J. Am. Chem. Soc.*, **101**, 5266 (1979).

[37] M.A. Castro, A.E. Roitberg, F.D. Cukiernik. *Inorg. Chem.*, **47**, 4682 (2008).

[38] M.A. Castro, A.E. Roitberg, F.D. Cukiernik. *J. Chem. Theor. Comput.*, **9**, 2609 (2013).

[39] L. Rossi, C. Huck-Iriart, P.S. Antonel, F.D. Cukiernik. *Work in progress*.